Effect of strain relaxations on heteroepitaxial metal-on-metal island nucleation and superlattice formation: Fe on Cu(111)

N. N. Negulyaev,[1] V. S. Stepanyuk,[2] L. Niebergall,[2] P. Bruno,[2,3] W. Auwärter,[4,5] Y. Pennec,[4] G. Jahnz,[4] and J. V. Barth[4,5]

[1]*Fachbereich Physik, Martin-Luther-Universität, Halle-Wittenberg, Friedemann-Bach-Platz 6, D-06099 Halle, Germany*
[2]*Max-Planck-Institut für Mikrostrukturphysik, Weinberg 2, D-06120 Halle, Germany*
[3]*European Synchrotron Radiation Facility, BP 220, F-38043 Grenoble Cedex, France*
[4]*Department of Physics and Astronomy, University of British Columbia, AMPEL 2355 East Mall, Vancouver, British Columbia, Canada V6T 1Z4*
[5]*Physik Department E20, Technische Universität München, James-Franck-Str. 1, D-85748 Garching, Germany*

Recent theoretical and experimental studies indicate that strain relaxations induced at a substrate can substantially affect the shape of nanostructures during thin-film epitaxy. We reveal the influence of strain relaxations on the self-ordering of Fe adatoms on Cu(111) during low-temperature submonolayer deposition by complementary experimental and theoretical investigations. Combining kinetic Monte Carlo and first-principles density-functional theory calculations, we study the interplay between surface nanostructuring and strain relaxations at the Cu substrate. The comparison of our theoretical results with scanning tunneling microscopy observations reveals marked effects on the adatom nucleation because of the substrate strain relief. The modified energy landscape around Fe adatoms and small close-packed Fe clusters at short distances (<6 Å) opens up a slippage motion channel mediating the formation of iron dimers and compact aggregates.

PACS number(s): 68.37.Ef

I. INTRODUCTION

Atomic-scale investigation of surface nanostructure formation attracted widespread interest during the last two decades. Epitaxial growth of islands, superlattices, and thin films opens an opportunity to create atomic structures with novel physical and chemical properties.[1–6] Most cases of heteroepitaxy imply a lattice mismatch between deposit and subjacent materials that causes strain in both surface and epitaxial layers. Strain relaxations can have a substantial influence on the detailed growth scenario.

Theoretical studies of atomic diffusion on semiconductor surfaces [Si(001) and GaAs(001)] revealed that strain alters the mobility of adatoms[7,8] and changes the nucleation kinetics.[9] Generally, the interface intermixing can be expected in systems dominated by atomic mismatch.[10] Experiments with Ag adatoms on a Ag(111) substrate and on compressively strained Ag layers grown on Pt(111) demonstrated that surface diffusion and interlayer mass transport are very sensitive to the variation in in-plane lattice constant. The substantial decreasing of the surface diffusion barrier[11] and the activation energy of the interlayer mass transport[12] were observed on the strained Ag(111), compared to that on the unstrained substrate. It was demonstrated that strain has a profound effect on the substrate-mediated interaction between adatoms on (111) noble-metal surfaces.[13,14] Another important ramification of the lattice mismatch between a deposit and a substrate is strain-induced shape transitions in nanoislands, which were predicted by Tersoff and Tromp.[15] Müller *et al.*[16] demonstrated that strain relaxations in nanoislands may lead to the growth of ramified structures even at interfaces with square symmetry. Later on, it was found that strain changes the energy balance between hollow sites and bridge positions in the systems with a large lattice mismatch, such as Co on Pt(111).[17,18] These studies explicitly demonstrated that a delicate balance between the strain energy and the bond energy within the island atoms determines the shape of a growing structure. The concept of *mesoscopic* size-dependent mismatch was introduced,[19,20] which allowed explanation of size-dependent atomic relaxations in nanoislands and details of atomic diffusion on strained surfaces.

Theoretical and experimental studies identified that the concept of mesoscopic misfit is crucial for the understanding of atomic kinetics and nucleation during early stages of epitaxial growth. Molecular static (MS) calculations demonstrated that strain relaxations affect the shape of a substrate and nanoislands during homoepitaxy[21] and heteroepitaxy,[20] which changes details of atomic motion near adislands[22] and on top of them.[23] The interplay between mesoscopic relaxations and activation barriers of interlayer mass transport at the edges of Cu nanoclusters on Cu(111) was revealed.[24] Strain fields that originated in a Cu(001) substrate in the vicinity of embedded iron islands significantly decrease the values of activation barriers for atomic exchange.[25] Strain relaxations in cobalt nanoislands on Cu(001) lead to stress oscillations with a period of one atomic layer[26] and can induce "fast" diffusion of small Co clusters.[27] It was found that strain has a strong influence on the surface electronic structure of Cu(001) covered with nitrogen[28] and on the rates of chemical reactions on noble-metal surfaces.[29] The size-dependent mismatch between Si islands and Si substrate was revealed to be a driving force for a surface morphology above percolation.[30] Recent scanning tunneling spectroscopy measurements showed that the surface states over nanoscale islands are modified as the lateral size of an island changes.[31] Theoretical studies identified that the mechanism responsible for this effect is related to the size-dependent mesoscopic relaxations.[31] To the best of our knowledge, the direct observations of strain relaxations in nanoislands were performed only very recently by means of surface x-ray diffraction
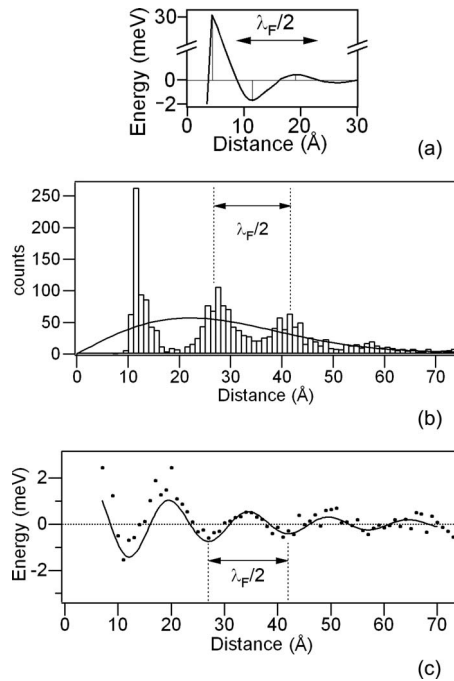
FIG. 1. (a) Schematic illustration of the electronic interaction between two Fe adatoms found in our calculations by means of the Korringa-Kohn-Rostocker Green's function method. The interaction between an Fe adatom and a close-packed Fe cluster of $n = 2-6$ atoms is qualitatively the same as the interaction between two adatoms. (b) Histogram of experimentally observed NN distances of Fe adatoms on Cu(111) ($T = 12$ K, $\Theta = 0.0016$ ML). The oscillatory distribution is induced by the substrate-mediated long-range interaction and clearly deviates from a random site occupation represented by the solid curve. (c) The interaction energy between two Fe adatoms as a function of distance as extracted from (b) (see text for discussion) nicely reflects *ab initio* calculations in (a).

measurements.[32,33] These remarkable investigations confirmed the concept of mesoscopic misfit, which governs the shape of clusters and a substrate in their vicinity.

In this paper we concentrate on the important ramification of strain relaxations: their influence on the nucleation of adatoms during early stages of thin-film epitaxy. When metal substrates such as Ag(111) or Cu(111) are employed, the balance of long-range interactions (LRI) mediated by the surface-state electrons[34–36] and short-range repulsions must be carefully assessed [Fig. 1(a)]. On Cu(111) attempts to create adatom superlattices exploiting the LRI have been reported[37,38] but mesoscale regularity was not achieved. *Ab initio* calculations suggest short-range repulsive barriers in the 20–80 meV range.[13,14,39,40] This represents a decisive factor in delaying nucleation to markedly higher coverages than anticipated in classical nucleation and growth models,[13,39,41,42] and can explain small apparent diffusion prefactors deduced therewith.[43] An approximate interpolation scheme indicates an adatom-adatom potential repulsive energy in the 10–14 meV range for Cu/Cu(111).[44] On the other hand, recent scanning tunneling microscope (STM) observations showed that on Ag(111) cerium adatoms readily form regular superlattices with 32 Å periodicity at $T = 3.9$ K,[45–47] and that the same substrate patterned with a supramolecular

grating can be used to stabilize Fe or Co atomic strings with 25 Å next-neighbor spacing.[48] Self-aligning Co atoms were also recently reported for an In modified Si(111) surface.[49] Further STM observations for molecular adsorbates indicate that additional electrostatic interaction terms may interfere in molecular long-range ordered superlattices.[50,51]

In this paper we focus on the low-temperature self-ordering of Fe adatoms on Cu(111) in a low-coverage regime. The behavior of Fe adatoms is studied both experimentally (by means of STM measurements) and theoretically [using kinetic Monte Carlo (kMC) simulations based on calculated activation barriers for atomic diffusion]. Our experimental observations indicate a surprisingly high nucleation density of compact Fe clusters following deposition and annealing procedures. The observations raise the question whether this effect is due to strain relaxations induced at a surface around Fe adsorbates or rather caused by the electronic effects (i.e., direct interaction between Fe adsorbates). Combining kMC simulations and first-principles density-functional theory (DFT) calculations, we unambiguously demonstrate that the driving force behind the observed phenomenon is strain relaxations in the substrate. We reveal the interplay between relaxations of a substrate and nucleation density of adsorbate Fe clusters.

In essence, we demonstrate an appreciable modification of the short-range interaction with a reduced migration barrier around Fe adatoms at short distances (<6 Å), which opens up a channel for additional low-temperature adatom displacements and promotes aggregation events. This represents a slippage motion or adatom funneling under conditions where monomer migration on the homogenous substrate atomic lattice is frozen in. Our interpretation is consistent with earlier field-ion microscopy observations of iridium adatoms on Ir(111),[52,53] but at variance with the data interpretation regarding silver atoms on Pt(111), where an analysis of the nucleation island densities suggested the complete absence of transient motions.[54] Compared to the adsorption of rare gases or molecular species where kinetic-energy dissipation goes along with frequently long-distance nonthermal precursor motions,[55–64] the range of the present hops with reduced barriers is limited to a distance of two substrate lattice constants.

The remainder of the paper has the following structure. In Sec. II we describe the experimental procedure. In Sec. III we discuss the observed morphology of Fe on Cu(111) at very low deposition coverage and present theoretical model which is used for the large-scale simulations of a self-ordering of Fe adatoms on a Cu(111) surface. In Sec. IV we compare the experimentally observed nucleation density of close-packed Fe clusters with the results of kMC simulations and demonstrate the influence of strain relaxations on the self-ordering.

II. EXPERIMENTAL

Our experiments were performed in a custom-designed ultrahigh-vacuum system[65] equipped with a commercial low-temperature STM (Ref. 66) based on a design described elsewhere.[67] The Cu(111) single-crystal surface was cleaned

by repeated cycles of Ar$^+$ sputtering (800 eV) followed by annealing to 780 K. Fe atoms were evaporated from a home-made water-cooled cell by resistively heating a tungsten fila-ment surrounded by an Fe wire of high purity (99.998%). Our experimental setup allows direct access of the atomic beam to the sample placed in the STM. The incidence angle of the atomic beam equals 11° with respect to the surface plane. Fe was deposited with a typical coverage of 0.01–0.06 monolayer (ML) and rate of ∼0.045 ML/h onto the Cu(111) surface at a temperature of about 12 K. Prior to the measure-ments, the sample was annealed at two different tempera-tures, 12 or 17 K, during $t_{an} \sim 30$ min. All STM images are taken in constant current mode using electrochemically edged tungsten tips. In the figure captions V refers to the bias voltage applied to the sample. To avoid tip induced adatom motion, low tunneling currents and very low bias voltages ($V < 50$ mV) were applied.[68]

III. TOPOGRAPHIC OBSERVATIONS AND THEORETICAL MODEL

On the (111) noble-metal surfaces the electronic interac-tion between adsorbates has a strong impact on the atomic motion at low temperature.[13,14,37,38,40,42,45–47,69,70] We use DFT calculations by means of the Korringa-Kohn-Rostocker (KKR) Green's function method for adatoms and supported clusters[71,72] in the single-particle approximation[36,40,69] to ob-tain the electronic interaction potential between an Fe ada-tom and an Fe adsorbate of an arbitrary size n (i.e., another adatom or small close-packed cluster). Clusters of different sizes n (up to six Fe atoms[73]) are considered. The basic idea of the exploited method is a hierarchical scheme for the con-struction of the Green's function of nanostructures on a sur-face by means of successive applications of Dyson's equa-tion. The bulk, surface, and impurity problems are consequently treated with a perturbative approach. At each stage a fully self-consistent Green's function is obtained, which is then used as a reference for the next step. We treat a surface as a two-dimensional perturbation of an ideal bulk with a slab of vacuum. Taking into account the translational symmetry of the surface geometry, the Green's functions are formulated in momentum space. Adatom and small clusters are considered as a perturbation of a clean surface. These calculations are performed in real space. The computational details can be found in the previous investigations.[40,69,74]

Our systematic studies identify that the electronic interac-tion between an Fe adatom and an Fe cluster of $n = 2–6$ atoms is qualitatively the same as the interaction between two Fe adatoms:[40] it has an oscillatory behavior with a pe-riod of half Fermi wavelength of a Cu(111) surface $\lambda_F/2 = 15$ Å, and exhibits (i) the first repulsive barrier at 4–8 Å, (ii) the attractive part at 9–15 Å, and (iii) the second repul-sive part at 16–23 Å [Fig. 1(a)]. The calculated parameters of the adatom-adatom LRI potential are confirmed by our experimental observations. Following the procedure intro-duced in Ref. 38, the distribution of the nearest-neighbor (NN) distances between Fe adatoms [Fig. 1(b)] at very low coverage $\Theta = 0.0016$ ML was translated into the interaction energy [Fig. 1(c)]. The first minimum of −1.6 meV at 12 Å
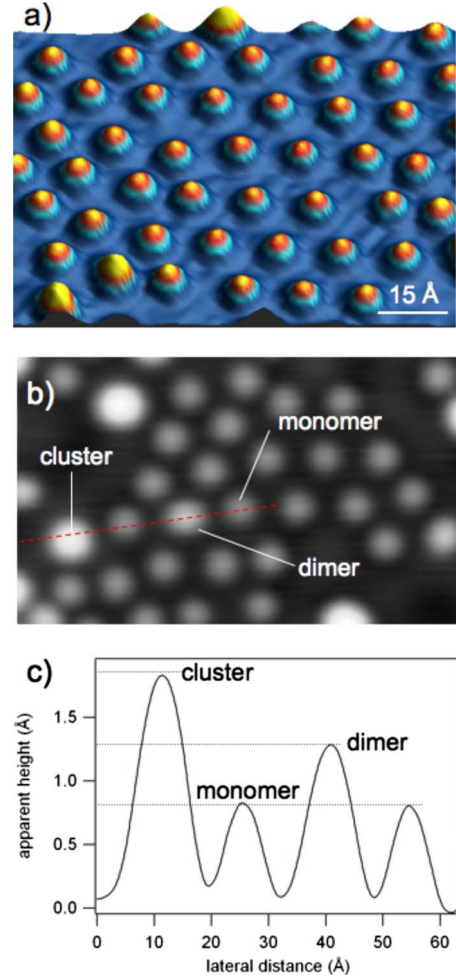

FIG. 2. (Color online) Topography of Fe on Cu(111). (a) Self-ordering of Fe adatoms into a quasihexagonal superstructure ($I = 0.2$ nA, $V = 25$ mV). (b) Detailed view highlighting the differ-ent observed Fe species: monomers, dimers, and clusters ($I = 0.16$ nA, $V = -59$ mV). (c) A height profile taken along the dashed line marked in (b) allows us to discriminate the three species by their characteristic apparent heights.

as well as the repulsive barrier of 0.8 meV at 18 Å nicely agree with the attractive and repulsive parts of the calculated adatom-adatom LRI potential, −1.8 and 0.6 meV, respec-tively. Accordingly, the nonrandom oscillatory distribution of Fe adatoms directly reflects the LRI between the adsorbates.

Figure 2 shows topographic images of the Cu(111) sur-face after Fe deposition and annealing at 12 K. Regions ex-hibiting a quasihexagonal ordering of protrusions and bare Cu(111) areas with brighter features are visible. The protru-sions are identified as single Fe adatoms and dimers while the features with a larger apparent height represent compact clusters of three or more Fe atoms. Figure 2(a) highlights a region, where the quasihexagonal ordering of Fe adatoms is well developed. The observed NN distances of 12–15 Å agree with the attractive part of the substrate-mediated po-tential, as presented in Fig. 1(a). A comparison of the adatom positions with a hexagonal mesh representing the Cu(111) surface atoms indicates that the Fe atoms are centered in equivalent hollow sites of the surface. While the quasihex-

agonal order shows that the low-temperature self-ordering of Fe atoms is enabled to some extent, an inspection of the large-scale topographic image reveals that the formation of clusters inhibits creation of a macroscopic-ordered Fe super-structure (see Sec. IV).

The main goal of our study is to prove that the formation of clusters is strongly promoted by strain relaxations origi-nated at the substrate around Fe adsorbates. This will be done by comparing the experimental morphology with the results of the kMC simulations. To perform this analysis, it is mandatory that single adatoms, dimers, and larger clusters be distinguished in the experimental data. In the surface area presented in Fig. 2(b), all these species are represented. The symmetries of the entities (round protrusion for monomers, ellipsoidal protrusions for dimers[75]) together with their char-acteristic apparent heights [displayed in the line profiles in Fig. 2(c)] allow for an unambiguous identification of the pro-trusions in the STM data.

In the following, we present a theoretical model, which is used for the large-scale atomic simulations. Kinetics of Fe adatoms on a Cu(111) surface at low temperature is investi-gated by means of the kMC method,[76] intensively applied in recent studies.[13,39,41,42,77–81] We consider two different ap-proaches to the calculation of activation barriers in the kMC simulations. Within the *first approach*, strain relaxations originated at the substrate around Fe adatoms and small close-packed Fe clusters are not involved. As a result, diffu-sion barriers for the atomic events are computed in the ideal geometry, i.e., taking into account electronic effects only. Within the *second approach* strain relaxations around Fe adatoms and small clusters are considered. Thus diffusion barriers are computed in a fully relaxed geometry. Compar-ing the difference in results obtained within two approaches, we reveal the interplay between the morphology of the epi-taxial adlayer and strain relaxations.

In our kMC simulations a Cu(111) surface is represented as a triangular lattice of fcc and hcp hollow sites with the separation $r_0/\sqrt{3}$ between the nearest sites, where r_0 =2.556 Å is the NN distance. The hop rate of an Fe adatom from site k to site j is calculated within the ratio $v_{k \to j}$ =$v_0 \exp(-E_{k \to j}/k_B T)$, where T is the substrate temperature, v_0 is the attempt frequency (which is considered to be 9 $\times 10^{11}$ Hz), and k_B is the Boltzmann factor. The hopping barrier for the atomic diffusion takes the following form:[13,42,78–81]

$$E_{k \to j} = E_D + 0.5(E_j - E_k). \qquad (1)$$

Here E_D is the diffusion barrier for an isolated adatom. Within the *first approach*, which does not consider strain relaxations in the substrate and involves electronic effects only, $E_{k(j)}$ in Eq. (1) is the sum of the electronic interaction of an Fe adatom located in site $k(j)$ with all other adsorbates [Fig. 1(a)]. If the number of adatoms in the system is equal to N, then for every kMC step $(3N+1)$ different events ($3N$ hops and the event associated with deposition of a new ada-tom, if the required coverage is not achieved) with the rates $v_1, v_2, \ldots, v_{3N+1}$ are possible. The time interval between two steps can be calculated:[76]

$$\tau = -\ln U / \sum_{i=1}^{3N+1} v_i, \qquad (2)$$

where U is a randomly distributed number in the interval (0, 1).

We employ MS calculations in order to (i) obtain diffu-sion barrier E_D [Eq. (1)] and (ii) describe strain relaxations at the substrate in the vicinity of Fe adsorbates. Many-body interatomic potentials formulated in the second moment ap-proximation of the tight-binding approach[82,83] are exploited for the system of Fe and Cu atoms. The parameters of po-tentials are taken from our previous works.[25,84] These studies and investigations of other related systems[22–24,85–89] demon-strated that the interatomic potentials constructed as de-scribed above provide a good approximation for atomic dis-placements found in *ab initio* calculations. Recent studies showed that one can use MS method with *ab initio* based interatomic potentials in order to obtain activation barriers for relevant atomic events, which are used as input in the kMC simulations.[90–95] In our MS simulations positions of Fe and Cu atoms are determined in a fully relaxed geometry. The slab consists of ten layers with 1840 atoms in each layer. Two bottom layers are fixed and the periodic boundary con-ditions are applied in a surface plane. The cutoff radius for the interatomic potentials is set to 6.0 Å.

The MS calculations show that the tracer diffusion barrier E_D of an individual Fe adatom is 28.5 meV if the hop from fcc to hcp hollow site takes place, and 26.6 meV for the opposite transition. We performed systematic experimental studies of the diffusion rate v of isolated Fe monomers as a function of time and temperature T by tracing their trajectory on consecutive STM images taken from the same surface area. The jump rate demonstrates perfect Arrhenius behavior shown in Fig. 3(a). From our experimental data we derive the energy barrier E_D and the attempt frequency v_0 for a single Fe adatom on Cu(111): 22 ± 7 meV and $1 \times 10^{10 \pm 2}$ Hz, respectively. The experimental value of E_D is within the error of the calculated one.

In order to reveal basic peculiarities of $E_{k \to j}$ [see Eq. (1)] as a function of separation r, we consider a system of two Fe adatoms. In Fig. 3(b) we schematically demonstrate a diffu-sion path of an Fe adatom toward another Fe adatom. Num-bers denote the elementary hops of the migrating adatom. Figure 3(c) (black curve) illustrates the potential-energy path $E_{k \to j}(r)$ of the migrating Fe adatom along the trajectory shown in Fig. 3(b). This curve is the result of summation of (i) the energy profile of a single diffusing Fe adatom and (ii) the electronic interaction potential between two Fe adatoms [Fig. 1(a)]. The approaching Fe adatom has to overcome the total barrier E_B of 59 meV arising at r_B=4.8 Å to form a dimer. The aggregation always takes place when the distance between two adatoms r is less than the radii of the capture zone r_B. The magnitude of r_B (together with E_B) sets the probability of nucleation at incoming flux F, and given cov-erage Θ and temperature T.

Now we turn to the details of the *second approach*, which considers kinetics of Fe atoms on a Cu(111) surface in the presence of strain relaxations around Fe adatoms and small
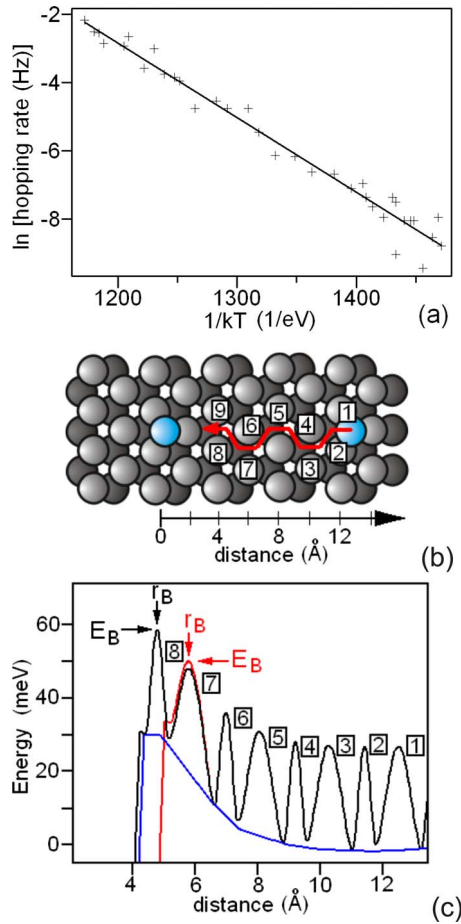
FIG. 3. (Color online) (a) Arrhenius plot of the experimental hopping rate of Fe adatoms on Cu(111). The fit (solid line) yields a diffusion barrier of 22 ± 7 meV and an attempt frequency of $1 \times 10^{10 \pm 2}$ Hz. (b) Illustration of a migration path of an Fe adatom toward an Fe adsorbate (another adatom). (c) The potential-energy landscape of an Fe adatom approaching another Fe adatom on Cu(111) in the presence (red color) and in the absence (black color) of strain relaxations, respectively. At $r > 6$ Å the effect of the mesoscopic relaxations is negligibly small; therefore the two curves coincide. The blue curve represents the electronic interaction between two Fe adatoms (Ref. 40).

Fe clusters. Deformation of the substrate leads to elastic interaction between the adsorbates.[96–98] Previous studies demonstrated that the energy of elastic interaction between two Fe adatoms at intermediate separations (7–20 Å) (Ref. 84) is one order less than the magnitude of the electronic interaction energy at the corresponding distances.[40] Thus at $r \geq 7$ Å we can safely exclude the effect of strain relaxations on diffusion barriers $E_{k \to j}(r)$. At short separations ($r \leq 6$ Å) the approaching adatom is located in the area where the substrate is substantially deformed due to the presence of the second Fe adatom. Displacement of substrate Cu atoms located in the vicinity of an Fe adatom from their ideal positions on a clean Cu(111) surface can reach 0.1–0.3 Å.[99]

In order to deduce the effect of strain relaxations on diffusion barriers at $r \leq 6$ Å, we rely on the following calculation procedure, which employs the MS simulations with the interatomic potentials for a system of Cu and Fe atoms.[25,84]

First, we place the migrating adatom in different hollow sites, as it is shown in Fig. 3(b), and compute the energy difference $\Delta E_R(r) = E_R(r) - E_R(\infty)$ as a function of adatom-adatom separation r in a fully relaxed geometry. Here $E_R(r)$ is the total energy of the slab with adatoms, corresponding to the distance r between two adatoms. Evidently, $\Delta E_R(r)$ is the interaction energy between two Fe adatoms, which includes both electronic and elastic effects. Next, we calculate the energy difference $\Delta E_I(r) = E_I(r) - E_I(\infty)$ as a function of adatom-adatom separation r in an ideal geometry [where $E_I(r)$ is the total energy of the slab with adatoms in an ideal geometry]. $\Delta E_I(r)$ is the interaction energy between two Fe adatoms, which involves electronic effects only. Thus, the difference $\quad H(r) = \Delta E_R(r) - \Delta E_I(r) = E_R(r) - E_R(\infty) - E_I(r) + E_I(\infty)$ is the interaction energy introduced by the surface deformation only. Note that if $r \geq 7$ Å, then $\Delta E_I(r) = 0$, and $H(r)$ is just the energy of elastic interaction.[84,96–98]

Thus, in the second approach the hopping barrier for the atomic diffusion takes the following form for the "adatom-adsorbate" separations $r \leq 6$ Å:

$$E_{k \to j} = E_D + 0.5(E_j - E_k) + 0.5(H_j - H_k). \quad (3)$$

Here $H_{k(j)}$ is the interaction energy between an Fe adatom located in site $k(j)$ and the adsorbate, which is caused by strain relaxations. For the larger separations ($r > 6$ Å) Eq. (1) is used.

Figure 3(c) (red curve) illustrates the potential-energy path $E_{k \to j}(r)$ of an Fe adatom migrating toward another Fe adatom along the trajectory shown in Fig. 3(b) in the presence of strain relaxations. This curve is the result of summation of (i) the energy profile of a single diffusing Fe adatom, (ii) the electronic interaction energy between two Fe adatoms [Fig. 1(a)], and (iii) the interaction energy $H(r)$ caused by the deformation of the substrate. We note that the presence of strain relaxations (i) decreases the total-energy barrier E_B for a dimer formation (50 vs 59 meV for the ideal surface) and (ii) increases the radii of the capture zone r_B (5.8 vs 4.8 Å for the ideal surface). This result suggests that strain relaxations could increase the probability of nucleation.

Following the procedure described above, we have examined the total-energy paths $E_{k \to j}(r)$ of an Fe adatom approaching close-packed clusters of $n = 2-6$ atoms. The corresponding cluster configurations and migration trajectories are depicted in Fig. 4. We have found that in all cases the general trend is the same: (i) strain relaxations can be excluded at intermediate separations ($r = 7-20$ Å) since the elastic interaction adatom-cluster is substantially less than the LRI at the corresponding distances; (ii) the magnitude of E_B decreases by 5–10 meV and (iii) the radii of the capture zone r_B is shifted from 4.8 to 5.8 Å on the strained substrate. For instance, when an Fe adatom migrates toward the close-packed dimer ($n = 2$) along the direction perpendicular to its axis [Fig. 4(a)], the magnitude of E_B equals to 47 meV in the presence of strain relaxations and 54 meV on an ideal surface. The corresponding values for a compact trimer [$n = 3$, Fig. 4(b)] are 42 and 50 meV, respectively; for a cluster of four atoms [Fig. 4(c)] −38 and 40 meV; for five atoms [Fig. 4(d)] −43 and 48 meV; for six atoms [Fig. 4(e)] −44 and 53 meV.
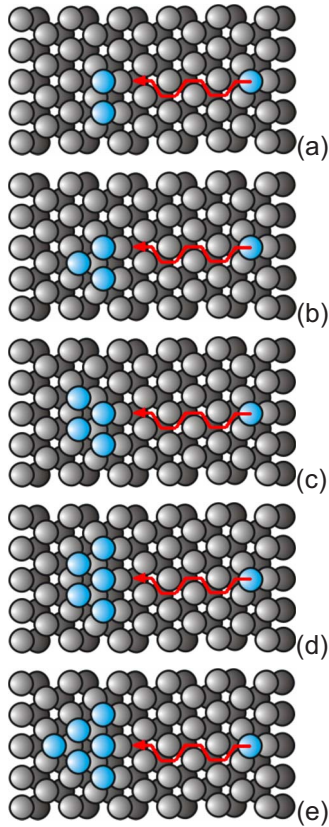
FIG. 4. (Color online) Migration paths of Fe adatom toward compact Fe clusters of two to six atoms.

Our experimental measurements prompt that Fe dimers are mobile within the range of temperatures considered. In Fig. 5(a) we show a set of STM images of an Fe dimer, which exhibits rotation observed at 12 K. The MS simulations support this finding and indicate that diffusion of dimers is possible. The energy difference between fcc and hcp stackings of an Fe dimer is $\Delta E = 4.5$ meV with the fcc stacking energetically more stable. At $T \sim 12$ K the probability to find an Fe dimer with a fcc stacking is $\exp(\Delta E/k_B T)$ ~ 100 times higher than that one with a hcp stacking. Hence the majority of dimers are located in fcc hollow sites. Our MS calculations identify that such Fe dimer may rotate around the center of mass of an underlying Cu atom with the
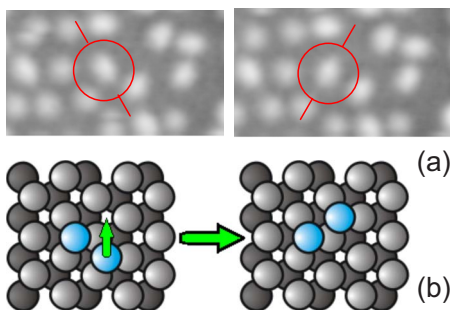

FIG. 5. (Color online) (a) STM image of an Fe dimer, which changes its orientation ($I = 0.07$ nA, $V = -25$ mV). (b) The MS calculations indicate that this rotation requires an activation energy 6 meV.
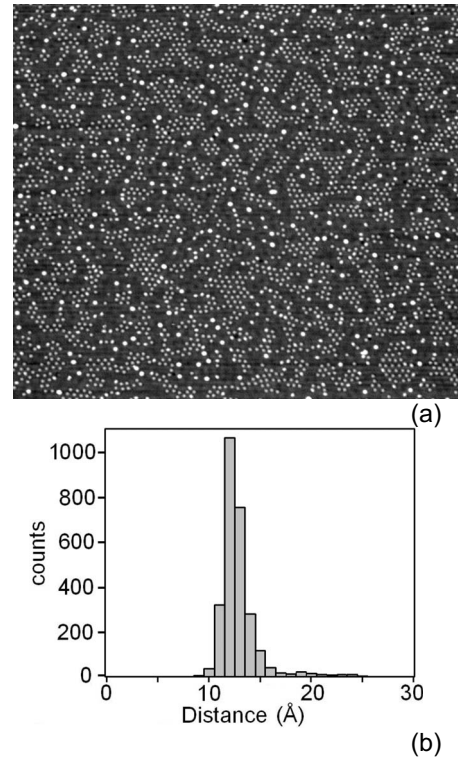

FIG. 6. (a) Experimentally observed topography of Fe on Cu(111). The experimental conditions during deposition are: $T = 12$ K, $\Theta = 0.021$ ML, $F = 0.045$ ML/h, annealing time is 30 min. The area 100×88 nm^2 is demonstrated. Bright spots correspond to the close-packed Fe clusters of three and more atoms. $I = 0.12$ nA, $V = 25$ mV. (b) The NN distribution function corresponding to the experimentally observed morphology (a).

barrier of 6 meV [Fig. 5(b)]. In the given experimental situation, the dimer rotation might be also influenced by neighboring adatoms.[75] Close-packed clusters of three and more Fe adatoms are immobile, as far as activation barriers for their diffusion exceed 0.1 eV.

Based on the results of this section, in the following we present the kMC simulations of the self-ordering of Fe adatoms using two different approaches, with and without strain relaxations. We compare the results of computer simulations with the experimental measurements. We essentially concentrate on the formation of immobile compact Fe clusters consisting of three and more atoms, and investigate their nucleation density at different experimental conditions (coverage and annealing temperatures). Our kMC simulations are performed in a cell of 60×60 nm^2. The periodic boundary conditions are applied along both plane directions.

IV. KMC SIMULATIONS VERSUS EXPERIMENTAL CLUSTER DENSITIES

In this section we compare the results of our experimental and theoretical studies on the self-ordering of Fe adatoms on a Cu(111) surface and discuss them. Figure 6(a) demonstrates the experimentally observed morphology of a Cu(111) surface covered by $\Theta = 0.021$ ML of Fe. Deposition of Fe adatoms took place at $T = 12$ K; after deposition the sample

is kept at 12 K during annealing time (about 30 min). Fe adatoms and dimers are organized into large dilute hexagonal islands with the interatomic spacing of ~12 Å [see NN distribution function in Fig. 6(b)]. These nanostructures are stabilized by the first local minimum of the LRI potential [Fig. 1(a)].[37,38,40,45–47,69,79,81] Aggregation of adatoms is hindered by the repulsive ring of the LRI potential arisen at r_B [Fig. 3(c)], and there are mostly isolated adatoms. The bright spots in Fig. 6(a) correspond to small close-packed Fe clusters (trimers, tetramers). We found that their concentration is about 0.016 nm^{-2} while the concentration of dimers equals to 0.046 nm^{-2}. The existence of immobile compact clusters prevents self-ordering of randomly distributed atoms into a macroscopic-ordered superlattice.[38,79,81] Formation of close-packed clusters takes place via two different mechanisms. Two Fe atoms landed during deposition at separation $r < r_B$ [radii of the capture zone, see Fig. 3(c)] forming a dimer. Furthermore, a couple of Fe adatoms landing at $r > r_B$ may nucleate if their thermal energy is enough to overcome the repulsive barrier E_B.

Following the experimental conditions we perform the kMC simulations by means of two different approaches described in the previous section.[100] We reveal that self-ordering of Fe adatoms into dilute nanoislands stabilized by the LRI takes place independently, whether strain relaxations are involved or not. However, we find a pronounced difference in the densities of close-packed clusters, obtained within two approaches. To clarify this point, we extract the cluster-size distribution from our theoretical data. On a fully relaxed substrate the density of dimers and larger clusters is found to be 0.049 and 0.015 nm^{-2}, respectively. These numbers are in an agreement with the experimental values. However, on an ideal surface the corresponding values are 0.047 and 0.006 nm^{-2}. We note that the second value is essentially lower than the density of close-packed clusters observed in

the experiment. Therefore we conclude that strain relaxations in the vicinity of Fe adsorbates have a profound effect on nucleation density, increasing the probability of cluster formation.

It is important to note that compact clusters of three (or more) Fe atoms tend to be located at the periphery of dilute hexagonal nanoislands stabilized by the LRI [Fig. 6(a)]. In order to understand the origin of this phenomenon we computed binding energies associated with two systems presented in Fig. 7(a). To obtain the binding energy of the system we sum up the LRI between all adsorbates. Both of the systems from Fig. 7(a) consist of the same types of adsorbates (six single atoms and a trimer), organized in a hexagonal nanoisland. Configuration A corresponds to the case when the trimer is located inside a dilute nanoisland; the binding energy associated with this system equals to −18.0 meV. Configuration B is related to the case when the trimer is at the periphery of a nanoisland; the binding energy
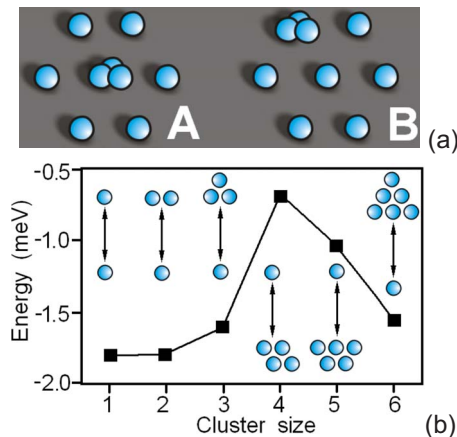

FIG. 7. (Color online) (a) Two hexagonal nanoislands stabilized by the first minimum of the LRI potential [Fig. 1(a)]. Both of them consist of six individual adatoms and a trimer. In case A the trimer is located at the center of a nanoisland while in case B the trimer is located at the periphery of a nanoisland. The separation between the adsorbates in hexagons is 12 Å. Configuration B is energetically more favorable than A (see text). (b) The LRI adatom cluster at $r \approx 12$ Å (the first minimum of the interaction energy) as a function of a cluster size n.
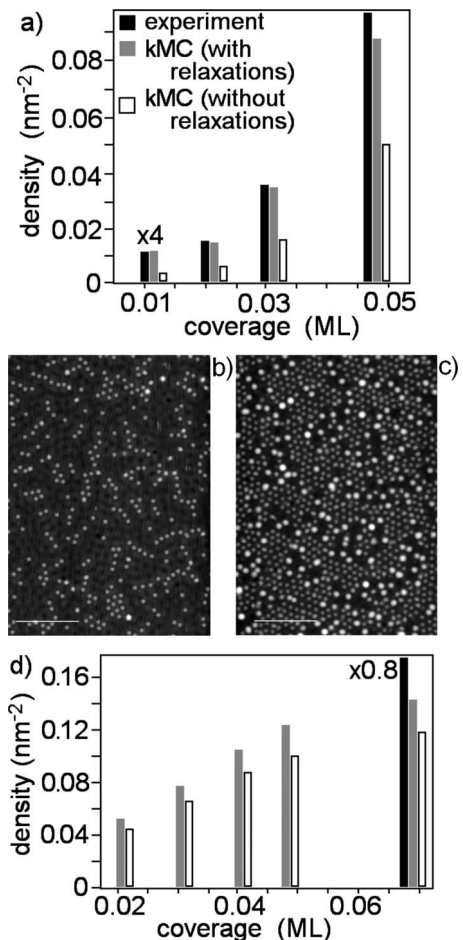

FIG. 8. The density of immobile Fe nanoislands as a function of coverage at annealing temperatures of (a) 12 and (d) 17 K. The data corresponding to 0.011 ML in (a) and 0.068 ML in (d) are rescaled by factors of 4 and 0.8, respectively. The STM images in (b) and (c) (scale bar of 12 nm) represent the surface morphology for the lowest ($I=0.11$ nA, $V=25$ mV) and the highest ($I=0.1$ nA, $V=25$ mV) coverage in (a). The experimental data in (d) are available not for all range of coverages considered in our theoretical calculations.

is found to be −19.2 meV. Thus, hexagonal structure with a trimer located at the periphery is energetically more stable than a nanoisland with a trimer in the center. In order to explain the difference in the binding energies associated with the configurations *A* and *B* [Fig. 7(a)], in Fig. 7(b) we plot the depth of the first minimum *B* of the LRI adatom cluster [Fig. 1(a)] as a function of cluster size *n*. This function exhibits nonmonotonic behavior, and a system of two Fe adatoms has the strongest attractive interaction among all system adatom clusters. Thus it is energetically favorable for Fe adatoms to be surrounded by monomers, forcing compact clusters to be located at the periphery of dilute nanoislands stabilized by the LRI.

Now we study the effect of strain relaxations on nucleation at different coverages and annealing temperatures. In Fig. 8(a) we plot the density of immobile clusters (≥3 atoms) at annealing temperature of 12 K as a function of the coverage. Four different coverages are considered: 0.011, 0.021, 0.031, and 0.048 ML. One can see that the concentration of immobile clusters measured in the experiment and that obtained within the kMC simulations on a fully relaxed substrate are close together. The nucleation density of clusters found in the kMC simulations in the absence of strain relaxations is significantly lower than the corresponding experimental values. The typical morphologies of a Cu(111) surface for the lowest (0.011 ML) and the highest (0.048 ML) coverages are demonstrated on Figs. 8(b) and 8(c).

Our studies give a clear evidence that the effect of mesoscopic relaxations around Fe adsorbates on the morphology of epitaxial layer becomes less pronounced at the elevated annealing temperatures. As the temperature increases, the influence of the repulsive barrier at 4–8 Å [Fig. 1(a)] on adatom diffusion becomes smaller, and the magnitude E_B and the position r_B of the repulsive ring [Fig. 3(c)] play a less prominent role. In order to demonstrate this, we performed a set of calculations at annealing temperature of 17 K and five different coverages (0.021, 0.031, 0.041, 0.048, and 0.068 ML). The results of our kMC simulations are presented in Fig. 8(d). The nucleation densities obtained without strain relaxations are rather close to those found in the presence of relaxations, in contrast to the case of annealing temperature of 12 K. The relative difference is 10–20 %, depending on the coverage. We also measured experimentally the nucleation density at the highest calculated coverage (0.068 ML) and plot the corresponding value in Fig. 8(d). A reasonable agreement between this value and the corresponding nucleation density found in the simulations in the presence of strain relaxations indicates the applied kMC model properly describes growth of Fe/Cu(111).

V. CONCLUSIONS

We have presented a combined experimental and theoretical investigation regarding the effect of strain relaxations in heteroepitaxial metal-on-metal nucleation and growth scenarios. Considering low-temperature self-ordering of Fe adatoms on Cu(111), we have demonstrated that strain relaxations induced in the substrate can have a pronounced effect on the energy landscape near the adsorbates. Our studies for different temperatures and coverages have identified that strain relaxations substantially increase the probability of close-packed cluster formation during the early stages of metal-to-metal epitaxial growth. Notably the expression of a regular adatom superlattice is obstructed. Results of our studies explicitly prove that substrate relaxations represent a key factor affecting atomic self-ordering and open a short-range (≤6 Å) slippage motion channel for adatom displacement leading to unexpectedly high island nucleation densities. It is suggested that these insights are of general relevance for morphology control of heteroepitaxial systems and represent a sensitive factor in the engineering of regular atomic or molecular superlattices stabilized by long-range interactions.

[1] Z. Y. Zhang and M. G. Lagally, Science **276**, 377 (1997).

[2] H. Brune, Surf. Sci. Rep. **31**, 121 (1998).

[3] F. J. Himpsel, J. E. Ortega, G. J. Mankey, and R. F. Willis, Adv. Phys. **47**, 511 (1998).

[4] V. A. Shchukin and D. Bimberg, Rev. Mod. Phys. **71**, 1125 (1999).

[5] J. W. Evans, P. A. Thiel, and M. C. Bartelt, Surf. Sci. Rep. **61**, 1 (2006).

[6] J. V. Barth, G. C. Costantini, and K. Kern, Nature (London) **437**, 671 (2005).

[7] S. V. Ghaisas, Surf. Sci. **223**, 441 (1989).

[8] C. Roland and G. H. Gilmer, Phys. Rev. B **46**, 13428 (1992).

[9] C. Ratsch and A. Zangwill, Appl. Phys. Lett. **63**, 2348 (1993).

[10] J. Tersoff, Phys. Rev. Lett. **74**, 434 (1995).

[11] H. Brune, K. Bromann, H. Röder, K. Kern, J. Jacobsen, P. Stoltze, K. Jacobsen, and J. Nørskov, Phys. Rev. B **52**, R14380 (1995).

[12] K. Bromann, H. Brune, H. Röder, and K. Kern, Phys. Rev. Lett. **75**, 677 (1995).

[13] K. A. Fichthorn and M. Scheffler, Phys. Rev. Lett. **84**, 5371 (2000).

[14] W. Luo and K. A. Fichthorn, Phys. Rev. B **72**, 115433 (2005).

[15] J. Tersoff and R. M. Tromp, Phys. Rev. Lett. **70**, 2782 (1993).

[16] B. Müller, L. Nedelmann, B. Fischer, H. Brune, J. V. Barth, and K. Kern, Phys. Rev. Lett. **80**, 2642 (1998).

[17] E. Lundgren, B. Stanka, M. Schmid, and P. Varga, Phys. Rev. B **62**, 2843 (2000).

[18] F. Meier, K. von Bergmann, P. Ferriani, J. Wiebe, M. Bode, K. Hashimoto, S. Heinze, and R. Wiesendanger, Phys. Rev. B **74**, 195411 (2006).

[19] R. Kern and P. Müller, Surf. Sci. **392**, 103 (1997).

[20] V. S. Stepanyuk, D. I. Bazhanov, A. N. Baranov, W. Hergert, P.

H. Dederichs, and J. Kirschner, Phys. Rev. B **62**, 15398 (2000).

[21] O. V. Lysenko, V. S. Stepanyuk, W. Hergert, and J. Kirschner, Phys. Rev. Lett. **89**, 126102 (2002).

[22] D. V. Tsivlin, V. S. Stepanyuk, W. Hergert, and J. Kirschner, Phys. Rev. B **68**, 205411 (2003).

[23] V. S. Stepanyuk, D. I. Bazhanov, W. Hergert, and J. Kirschner, Phys. Rev. B **63**, 153406 (2001).

[24] O. V. Lysenko, V. S. Stepanyuk, W. Hergert, and J. Kirschner, Phys. Rev. B **68**, 033409 (2003).

[25] R. C. Longo, V. S. Stepanyuk, W. Hergert, A. Vega, L. J. Gallego, and J. Kirschner, Phys. Rev. B **69**, 073406 (2004).

[26] D. Sander, S. Ouazi, V. S. Stepanyuk, D. I. Bazhanov, and J. Kirschner, Surf. Sci. **512**, 281 (2002).

[27] R. A. Miron and K. A. Fichthorn, Phys. Rev. B **72**, 035415 (2005).

[28] D. Sekiba, K. Nakatsuji, Y. Yoshimoto, and F. Komori, Phys. Rev. Lett. **94**, 016808 (2005).

[29] D. Sekiba, Y. Yoshimoto, K. Nakatsuji, Y. Takagi, T. Iimori, S. Doi, and F. Komori, Phys. Rev. B **75**, 115404 (2007).

[30] R. Dana and Y. Manassen, Europhys. Lett. **79**, 16001 (2007).

[31] M. V. Rastei, B. Heinrich, L. Limot, P. A. Ignatiev, V. S. Stepanyuk, P. Bruno, and J. P. Bucher, Phys. Rev. Lett. **99**, 246102 (2007).

[32] O. Mironets, H. L. Meyerheim, C. Tusche, V. S. Stepanyuk, E. Soyka, P. Zschack, H. Hong, N. Jeutter, R. Felici, and J. Kirschner, Phys. Rev. Lett. **100**, 096103 (2008).

[33] O. Mironets, H. L. Meyerheim, C. Tusche, V. S. Stepanyuk, E. Soyka, H. Hong, P. Zschack, N. Jeutter, R. Felici, and J. Kirschner, Phys. Rev. B **79**, 035406 (2009).

[34] T. L. Einstein and J. R. Schrieffer, Phys. Rev. B **7**, 3629 (1973).

[35] H. Lau and W. Kohn, Surf. Sci. **75**, 69 (1978).

[36] P. Hyldgaard and M. Persson, J. Phys.: Condens. Matter **12**, L13 (2000).

[37] J. Repp, F. Moresco, G. Meyer, K.-H. Rieder, P. Hyldgaard, and M. Persson, Phys. Rev. Lett. **85**, 2981 (2000).

[38] N. Knorr, H. Brune, M. Epple, A. Hirstein, M. A. Schneider, and K. Kern, Phys. Rev. B **65**, 115420 (2002).

[39] A. Bogicevic, S. Ovesson, P. Hyldgaard, B. I. Lundqvist, H. Brune, and D. R. Jennison, Phys. Rev. Lett. **85**, 1910 (2000).

[40] V. S. Stepanyuk, L. Niebergall, R. C. Longo, W. Hergert, and P. Bruno, Phys. Rev. B **70**, 075414 (2004).

[41] S. Ovesson, A. Bogicevic, G. Wahnström, and B. I. Lundqvist, Phys. Rev. B **64**, 125423 (2001).

[42] K. A. Fichthorn, M. L. Merrick, and M. Scheffler, Phys. Rev. B **68**, 041404(R) (2003).

[43] J. V. Barth, H. Brune, B. Fischer, J. Weckesser, and K. Kern, Phys. Rev. Lett. **84**, 1732 (2000).

[44] J. A. Venables and H. Brune, Phys. Rev. B **66**, 195404 (2002).

[45] F. Silly, M. Pivetta, M. Ternes, F. Patthey, J. P. Pelz, and W.-D. Schneider, Phys. Rev. Lett. **92**, 016101 (2004).

[46] M. Ternes, C. Weber, M. Pivetta, F. Patthey, J. P. Pelz, T. Giamarchi, F. Mila, and W.-D. Schneider, Phys. Rev. Lett. **93**, 146805 (2004).

[47] F. Silly, M. Pivetta, M. Ternes, F. Patthey, J. P. Pelz, and W.-D. Schneider, New J. Phys. **6**, 16 (2004).

[48] A. Schiffrin, J. Reichert, W. Auwärter, G. Jahnz, Y. Pennec, A. Weber-Bargioni, V. S. Stepanyuk, L. Niebergall, P. Bruno, and J. V. Barth, Phys. Rev. B **78**, 035424 (2008).

[49] C. Liu, T. Uchihashi, and T. Nakayama, Phys. Rev. Lett. **101**, 146104 (2008).

[50] I. Fernandez-Torrente, S. Monturet, K. J. Franke, J. Fraxedas, N. Lorente, and J. I. Pascual, Phys. Rev. Lett. **99**, 176103 (2007).

[51] T. Yokoyama, T. Takahasi, K. Shinozaki, and M. Okamoto, Phys. Rev. Lett. **98**, 206102 (2007).

[52] S. C. Wang and G. Ehrlich, Phys. Rev. Lett. **70**, 41 (1993).

[53] S. C. Wang and G. Ehrlich, Phys. Rev. Lett. **71**, 4174 (1993).

[54] H. Brune, G. S. Bales, J. Jacobsen, C. Boragno, and K. Kern, Phys. Rev. B **60**, 5991 (1999).

[55] J. C. Tully, Surf. Sci. **111**, 461 (1981).

[56] P. S. Weiss and D. M. Eigler, Phys. Rev. Lett. **69**, 2240 (1992).

[57] B. C. Stipe, M. A. Rezaei, and W. Ho, J. Chem. Phys. **107**, 6443 (1997).

[58] J. V. Barth, Surf. Sci. Rep. **40**, 75 (2000).

[59] J. V. Barth, T. Zambelli, J. Wintterlin, and G. Ertl, Chem. Phys. Lett. **270**, 152 (1997).

[60] T. Zambelli, J. Wintterlin, J. Trost, and G. Ertl, Science **273**, 1688 (1996).

[61] T. Zambelli, J. V. Barth, J. Wintterlin, and G. Ertl, Nature (London) **390**, 495 (1997).

[62] J. Yoshinobu, N. Tsukahara, F. Yasui, K. Mukai, and Y. Yamashita, Phys. Rev. Lett. **90**, 248301 (2003).

[63] T. Takaoka and T. Komeda, Phys. Rev. Lett. **100**, 046104 (2008).

[64] N. Tsukahara, K. Mukai, Y. Yamashita, and J. Yoshinobu, J. Chem. Phys. **128**, 054701 (2008).

[65] W. Auwärter, A. Schiffrin, A. Weber-Bargioni, Y. Pennec, A. Riemann, and J. V. Barth, Int. J. Nanotechnol. **5**, 1171 (2008).

[66] GMBH Createc, D-74391 Erligheim, Germany, URL: www.lt-stm.com.

[67] G. Meyer, Rev. Sci. Instrum. **67**, 2960 (1996).

[68] M. F. Crommie, C. P. Lutz, and D. M. Eigler, Science **262**, 218 (1993).

[69] V. S. Stepanyuk, A. N. Baranov, D. V. Tsivlin, W. Hergert, P. Bruno, N. Knorr, M. A. Schneider, and K. Kern, Phys. Rev. B **68**, 205410 (2003).

[70] H. F. Ding, V. S. Stepanyuk, P. A. Ignatiev, N. N. Negulyaev, L. Niebergall, M. Wasniowska, C. L. Gao, P. Bruno, and J. Kirschner, Phys. Rev. B **76**, 033409 (2007).

[71] K. Wildberger, V. S. Stepanyuk, P. Lang, R. Zeller, and P. H. Dederichs, Phys. Rev. Lett. **75**, 509 (1995).

[72] V. S. Stepanyuk, W. Hergert, K. Wildberger, R. Zeller, and P. H. Dederichs, Phys. Rev. B **53**, 2121 (1996).

[73] We found that the formation of close-packed clusters of more than six Fe atoms unlikely takes place under the experimental conditions considered within our study.

[74] L. Niebergall, G. Rodary, H. F. Ding, D. Sander, V. S. Stepanyuk, P. Bruno, and J. Kirschner, Phys. Rev. B **74**, 195436 (2006).

[75] K. Morgenstern and K.-H. Rieder, New J. Phys. **7**, 139 (2005).

[76] K. A. Fichthorn and W. H. Weinberg, J. Chem. Phys. **95**, 1090 (1991).

[77] S. Ovesson, A. Bogicevic, and B. I. Lundqvist, Phys. Rev. Lett. **83**, 2608 (1999).

[78] V. S. Stepanyuk, N. N. Negulyaev, L. Niebergall, R. C. Longo, and P. Bruno, Phys. Rev. Lett. **97**, 186403 (2006).

[79] J. M. Rogowska and M. Maciejewski, Phys. Rev. B **74**, 235402 (2006).

[80] M. Ziegler, J. Kröger, R. Berndt, A. Filinov, and M. Bonitz, Phys. Rev. B **78**, 245427 (2008).

[81] J. Hu, B. Teng, F. Wu, and Y. Fang, New J. Phys. **10**, 023033

(2008).

[82] V. Rosato, B. Guillope, and B. Legrand, Philos. Mag. A **59**, 321 (1989).

[83] F. Cleri and V. Rosato, Phys. Rev. B **48**, 22 (1993).

[84] R. C. Longo, V. S. Stepanyuk, and J. Kirschner, J. Phys.: Condens. Matter **18**, 9143 (2006).

[85] N. A. Levanov, V. S. Stepanyuk, W. Hergert, D. I. Bazhanov, P. H. Dederichs, A. A. Katsnelson, and C. Massobrio, Phys. Rev. B **61**, 2230 (2000).

[86] S. Pick, V. S. Stepanyuk, A. L. Klavsyuk, L. Niebergall, W. Hergert, J. Kirschner, and P. Bruno, Phys. Rev. B **70**, 224419 (2004).

[87] V. S. Stepanyuk, A. L. Klavsyuk, L. Niebergall, A. M. Saletsky, W. Hergert, and P. Bruno, Phase Transitions **78**, 61 (2005).

[88] R. A. Miron and K. A. Fichthorn, Phys. Rev. Lett. **93**, 128301 (2004).

[89] K. Sastry, D. D. Johnson, D. E. Goldberg, and P. Bellon, Phys. Rev. B **72**, 085438 (2005).

[90] R. Ferrando, F. Hontinfinde, and A. C. Levi, Phys. Rev. B **56**, R4406 (1997).

[91] R. Ferrando, F. Hontinfinde, and A. C. Levi, Surf. Sci. **402-404**, 286 (1998).

[92] C. Mottet, R. Ferrando, F. Hontinfinde, and A. C. Levi, Surf. Sci. **417**, 220 (1998).

[93] N. N. Negulyaev, V. S. Stepanyuk, P. Bruno, L. Diekhöner, P.

[94] O. V. Stepanyuk, N. N. Negulyaev, A. M. Saletsky, and W. Hergert, Phys. Rev. B **78**, 113406 (2008).

[95] C. H. Claassens, J. J. Terblans, M. J. H. Hoffman, and H. C. Swart, Surf. Interface Anal. **37**, 1021 (2005).

[96] K. H. Lau and W. Kohn, Surf. Sci. **65**, 607 (1977).

[97] V. I. Marchenko and A. Y. Parshin, Sov. Phys. JETP **52**, 129 (1980).

[98] L. E. Shilkrot and D. J. Srolovitz, Phys. Rev. B **55**, 4737 (1997).

[99] Displacements of Cu atoms of similar magnitudes were found in the previous studies. Even such small displacements substantially increase the rate of a Fe embedding in the vicinity of embedded Fe clusters on Cu(001) (Ref. 24) and lead to a strong variation in the occupation probability of hollow sites surrounding Cu clusters on Cu(111) (Ref. 21).

[100] In our simulations "current time" is calculated as a sum of time increments τ corresponding to each step of the kMC algorithm [see Eq. (2)]. During period of time Θ/F adatom self-assembly is simulated at temperature of 12 K simultaneously with deposition until the required coverage is achieved. During the next 30 min (annealing time t_{an}) only adatom dynamics is simulated at temperature either at 12 or 17 K, depending on the experimental conditions. Thus, the observation of surface morphology takes place in the moment of time $(\Theta/F + t_{an})$.